Sensors & Actuators: B. Chemical 364 (2022) 131815

Contents lists available at ScienceDirect

Sensors and Actuators: B. Chemical

journal homepage: www.elsevier.com/locate/snb

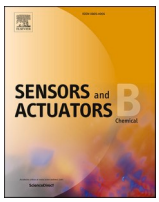

Electrochemical gas sensing module combined with Unmanned Aerial Vehicles for air quality monitoring

Patricia Arroyo [a], Jaime Gómez-Suárez [a], José Luis Herrero [b], Jesus Lozano [a,*]

[a] Department of Electric Technology, Electronics and Automation, University of Extremadura, Avda. de Elvas s/n, 06006 Badajoz, Spain
[b] Department of Computer and Telematics Systems Engineering, University of Extremadura, Avda. de Elvas s/n, 06006, Badajoz, Spain

ARTICLE INFO

Keywords:
Unmanned aerial vehicle
Air quality monitoring
Gas sensors
Electronic instrumentation
Data processing
Calibration

ABSTRACT

The issue of air pollution and the monitoring of air quality is a very serious problem in today's society. This problem is basically caused by human in activities related to industry, construction, transport, etc. High pollution values have become an important risk factor for the health of citizens. Measuring pollution for air quality control is not an easy task, as it requires highly specialized equipment, working under special conditions, which makes reference systems bulky and costly installations. To this must be added the disadvantages of measuring in areas with little or no accessibility. The aim of this work is to develop an unmanned aerial vehicle (UAV) equipped with low-cost sensors to monitor air quality both on the move and stationary in a position that is difficult to access. It is equipped with sensors for carbon monoxide (CO), ozone (O_3), nitrogen monoxide (NO) and nitrogen dioxide (NO_2) measurement. The electronic instrumentation has been developed in the laboratory for this application and it is optimized to minimize interference between the different devices. It also incorporates a pneumatic pump and a tube for air sampling outside the influence of the propellers. In this study, a series of measurements of the UAV were carried out at a stationary location next to a reference station in order to perform the calibration of the sensors. Once calibrated, a series of measurements have been made in motion. The experimental results show the accuracy of the measurements of the proposed prototype as well as its robustness in-flight measurements.

1. Introduction

The problem of air pollution is a matter of great relevance in the field of public health since it is the cause of a wide variety of diseases and is even responsible for a high number of deaths worldwide [1]. According to the EEA (European Environment Agency), nitrogen dioxide particles (NO_2) and ground-level ozone (O_3), are the pollutants that most significantly affect human health [2].

Nowadays, it is widely demonstrated that air pollution can cause disease and shorten life [3,4]. Exposure to high levels of pollution over long periods of time increases the severity of diseases and can cause from deterioration of the respiratory system to premature death [5]. The most common diseases caused by air pollution include ischemic heart disease [6], stroke [7], chronic obstructive pulmonary disease (COPD) [8], lung cancer [9], and can even lead to acute respiratory tract infections in children [10].

Because of the health implications of air pollutants, it is essential to detect them effectively. In recent decades, different alternatives have been proposed to carry out these measurements. In general, air pollution is monitored through ground stations offering very accurate measurements. However, they usually are very large, heavy and expensive devices [11] and do not allow to evaluate pollution at different heights [12], which is critical to understand how local or regional pollutants behave [13]. A different alternative employs balloons to detect the physicochemical characteristics of atmospheric layers [14]. The main advantages of this approach are that balloons can carry a large number of instruments and allow measurements to be taken with great reliability [15]. Nevertheless, they are expensive, difficult to control and have very limited mobility [16]. Satellites are also used to monitor the spatial distribution of air pollution [17]. However, this option is very expensive, it is not suitable when measurements of the same place need to be taken in short periods of time and in addition, the measurements obtained do not have a high vertical nor horizontal resolution [18]. In recent years, Unmanned Aerial Vehicles (UAVs) are being applied to measure environmental chemical compounds. In this sense, the use of multirotors is gaining special relevance, since they provide a large

* Corresponding author.
E-mail address: jesuslozano@unex.es (J. Lozano).

https://doi.org/10.1016/j.snb.2022.131815
Received 19 December 2021; Received in revised form 9 March 2022; Accepted 29 March 2022
Available online 6 April 2022

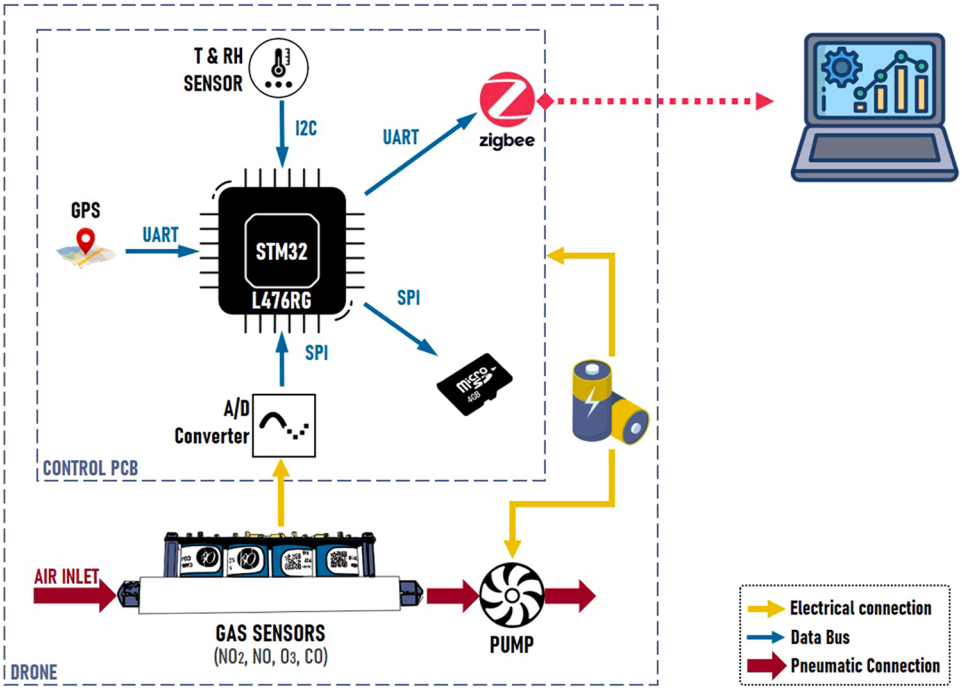

Fig. 1. Sampling and air quality measurement system components.

Fig. 2. Hexacopter and detail of the electronic system.

number of advantages, such as their ability to take measurements at different heights, the possibility of accessing hard-to-reach places, their easy handling and maneuverability and, in addition, they are vehicles that require a relatively low investment [19]. In recent years, several works have been proposed to address the challenge of detecting compounds in the air using multirotors. With this aim, different works have been published proposing the integration of different types of sensors into multirotors to detect atmospheric pollutants [20–23]. In this regard, to expand the number of atmospheric variables monitored from multirotors, a platform that integrates different types of sensors capable of measuring meteorological conditions, wind direction and atmospheric pollutants has been proposed [24]. On the other hand, the possibility of reducing air pollution using UAVs has also been studied and in this context, a UAV-based system has been adapted to measure and reduce air pollution by spreading a scrubbing solution comprising of H_2O_2 and HNO_3 in order to reduce the concentration of NO_2 in the air [25].

Regarding the choice of sensors, the use of low-cost gas sensors (LCS) has proven to be a good alternative to address problems in the field of atmospheric monitoring [26]. According to the sensor operation principle, there is a wide variety of technologies, the most commons being electrochemical sensors (EC), semiconductor metal oxide sensors (MOX sensors), non-dispersive infrared sensors (NDIR) or photoionization detectors (PID). Some authors such as [27] carry out an exhaustive study of the technology and the results that have been obtained with this type of sensors recently, showing that electrochemical gas sensors are the most common choice when it comes to monitoring CO, NO, NO_2 or O_3. In addition, they describe the charasteristic problems that arise when working with this type of sensors, such as cross-sensitivity, strong dependence on temperature and relative humidity, drift etc. Currently, low-cost sensors get better results when working in controlled laboratory conditions rather than working in the field, as shown [28]. For this reason, when working with low-cost sensors, it is common to resort to calibration algorithms that, with reference equipment, allow to adjust the sensors, previously calibrated by manufacturers in the laboratory, to work in the field. As a calibration tool, recent works [29,30] use Machine Learning algorithms such as Artificial Neural Networks, or Support Vector Machines. Once a good calibration model is obtained, new challenges can be addressed and in the last few years, there have been proposed novel approaches to detect especial situations in quemical sensing using UAVs. For instance, the source-receptor distance has be predicted even in a turbulence plume by applying low-pass differentiator filters for extracting transient features of gas sensor signals [31]. Another work has focused on monitoring dust particles at open-pit mine sites integrating opto-electrical dust sensors into UAVs to characterize blasting plumes in real time [32]. The use of electrochemical sensors embedded in unmanned aerial vehicles has also been applied for detecting and monitoring controlled brush fires [33]. Recently, a novel approach has developed an e-nose device integrated into UAVs for real-time odor quantification in wastewater treatment plants.

However, as it has been highlighted in a very comprehensive and updated review on chemical sensing and small drones [34], the application of unmanned aerial vehicles to monitor environmental chemical sensing entails new challenges that must be addressed. Specifically, it is of vital importance to consider the possible interferences between the different sensors used and the vehicle itself [35]. Electromagnetic interferences can seriously affect the operation of both systems, causing

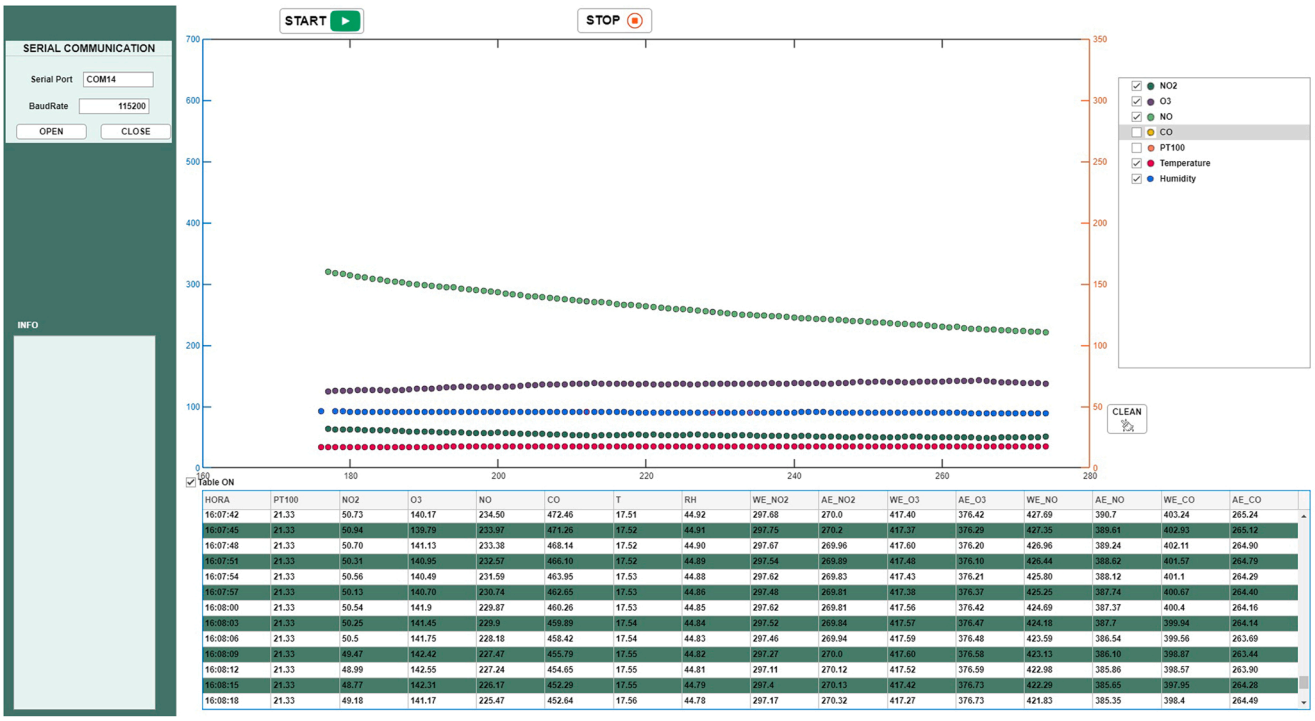

HORA	PT100	NO2	O3	NO	CO	T	RH	WE_NO2	AE_NO2	WE_O3	AE_O3	WE_NO	AE_NO	WE_CO	AE_CO
16:07:42	21.33	50.73	140.17	234.50	472.46	17.51	44.92	297.68	270.0	417.40	376.42	427.69	390.7	403.24	265.24
16:07:45	21.33	50.94	139.79	233.97	471.26	17.52	44.91	297.75	270.2	417.37	376.29	427.35	389.61	402.93	265.12
16:07:48	21.33	50.70	141.13	233.38	468.14	17.52	44.90	297.67	269.96	417.60	376.20	426.96	389.24	402.11	264.90
16:07:51	21.33	50.31	140.95	232.57	466.10	17.52	44.89	297.54	269.89	417.48	376.10	426.44	388.62	401.57	264.79
16:07:54	21.33	50.56	140.49	231.59	463.95	17.53	44.88	297.62	269.83	417.43	376.21	425.80	388.12	401.1	264.29
16:07:57	21.33	50.13	140.70	230.74	462.65	17.53	44.86	297.48	269.81	417.38	376.37	425.25	387.74	400.67	264.40
16:08:00	21.33	50.54	141.9	229.87	460.26	17.53	44.85	297.62	269.81	417.56	376.42	424.69	387.37	400.4	264.16
16:08:03	21.33	50.25	141.45	229.9	459.89	17.54	44.84	297.52	269.84	417.57	376.47	424.18	387.7	399.94	264.14
16:08:06	21.33	50.5	141.75	228.18	458.42	17.54	44.83	297.46	269.94	417.59	376.48	423.59	386.54	399.56	263.69
16:08:09	21.33	49.47	142.42	227.47	455.79	17.55	44.82	297.27	270.0	417.60	376.58	423.13	386.10	398.87	263.44
16:08:12	21.33	48.99	142.55	227.24	454.65	17.55	44.81	297.11	270.12	417.52	376.59	422.98	385.86	398.57	263.90
16:08:15	21.33	48.77	142.31	226.17	452.29	17.55	44.79	297.4	270.13	417.42	376.73	422.29	385.65	397.95	264.28
16:08:18	21.33	49.18	141.17	225.47	452.64	17.56	44.78	297.17	270.32	417.27	376.73	421.83	385.35	398.4	264.49

Fig. 3. Software programmed in Matlab for transferring the data from the UAV to the PC.

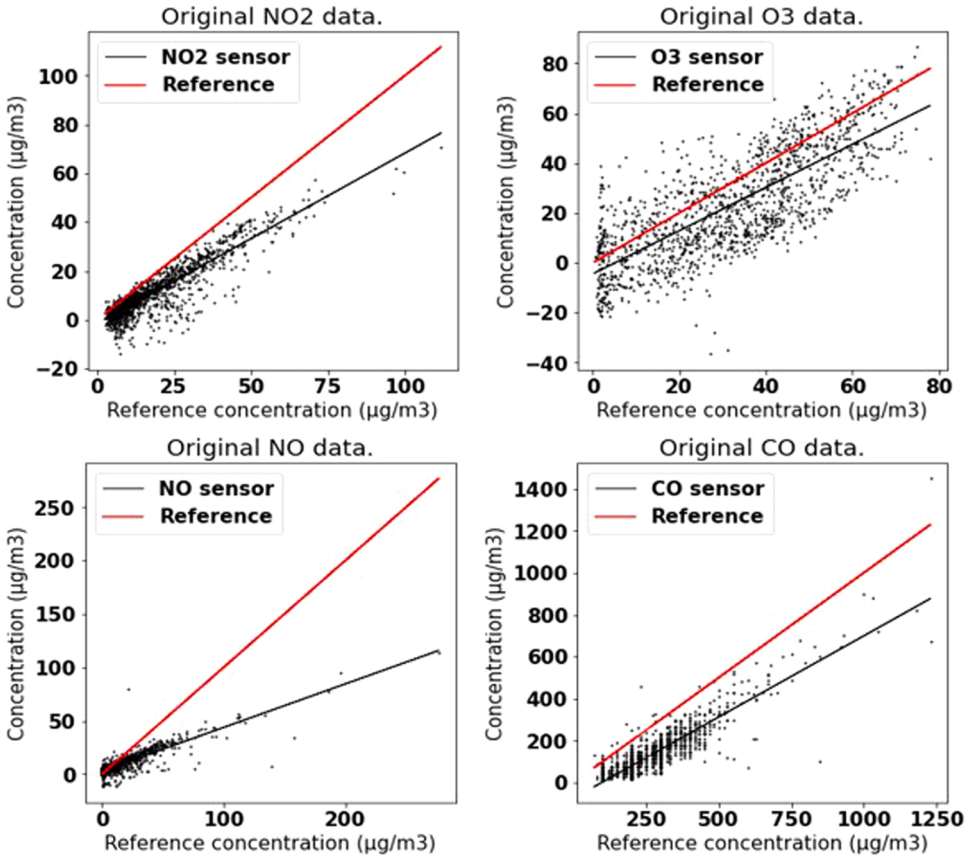

Fig. 4. Data from reference equipment against data from sensor array.

Table 1
Original data metrics.

Pollutant	MAE	MSE	R2	Mean
O_3	19.21	436.99	-0.26	31.38
NO_2	5.52	47.69	0.68	20.13
NO	5.44	77.54	0.67	13.45
CO	126.52	19,654.84	0.11	284.95

situations of risk not only for the vehicle but also for people in the vicinity. Interferences can also affect measurements taken by sensors, leading to erroneous results [36,37]. The calibration problem becomes even more complicated when these interferences are taken into account [38]. Authors such as [39] address this problem considering also UAV flight parameters when sensors are calibrated. Another important problem that must be analyzed is the location where sensors should be placed in the UAV since the downwash airflow produced by the propellers can seriously affect the measurements taken by the sensors [40, 41]. Furthermore, as propellers revolution speed increase, turbulence around the UAV becomes more significant, causing the dispersion of air compounds [42]. Several studies have been carried out focused on the selection of the best position to integrate LCS sensors into UAVs in order to precise detect compounds in the air. Experimental approaches show that better results are obtained when sensors are integrated into the lower part of the UAV instead of in its upper part [43]. Other works have been focused on the study of UAV downwash to find out the position airflow affects sensors the least [44].

The present work proposes an LCS device integrated into a multirotor, lightweight, low cost and low consumption, specifically designed for the detection of pollutants in the air. In addition, the problems resulting from both, electromagnetic interferences and downwash airflow generated by the propellers of the UAV, have been addressed. In the following sections, the measurement system will be described, the UAV will be explained in detail, as well as the integration of the measurement system in it. Next, four calibration algorithms will be proposed: Multiple Linear Regression (MLR), Artificial Neural Network (ANN), Random Forest (RF) and Support Vector Machine (SVR). These four techniques will be evaluated later by means of statistics that will allow choosing the method that works best so that, once the appropriate method is in place, the sensors can be calibrated. The results will then be presented before and after calibration. In addition, flights have been performed to check the stability and correct operation of the system to detect changes in pollutant concentrations. The results of these flights are shown in Section 3. Finally, Section 4 summarizes the main conclusions of this work.

Table 2
Metrics by algorithm. The best value is underlined.

Pollutant	MAE				MSE				R^2			
	MLR	ANN	RF	SVR	MLR	ANN	RF	SVR	MLR	ANN	RF	SVR
O_3	7.36	7.31	9.95	7.38	71.22	74.67	136.89	71.33	0.79	0.78	0.60	0.79
NO_2	2.10	2.03	2.56	2.74	7.27	6.93	10.29	11.23	0.94	0.95	0.93	0.92
NO	4.00	2.70	2.31	2.92	23.37	14.83	12.47	12.03	0.90	0.94	0.95	0.95
CO	39.35	52.60	46.38	45.35	2560.63	5687.55	3494.28	3464.52	0.79	0.53	0.71	0.71

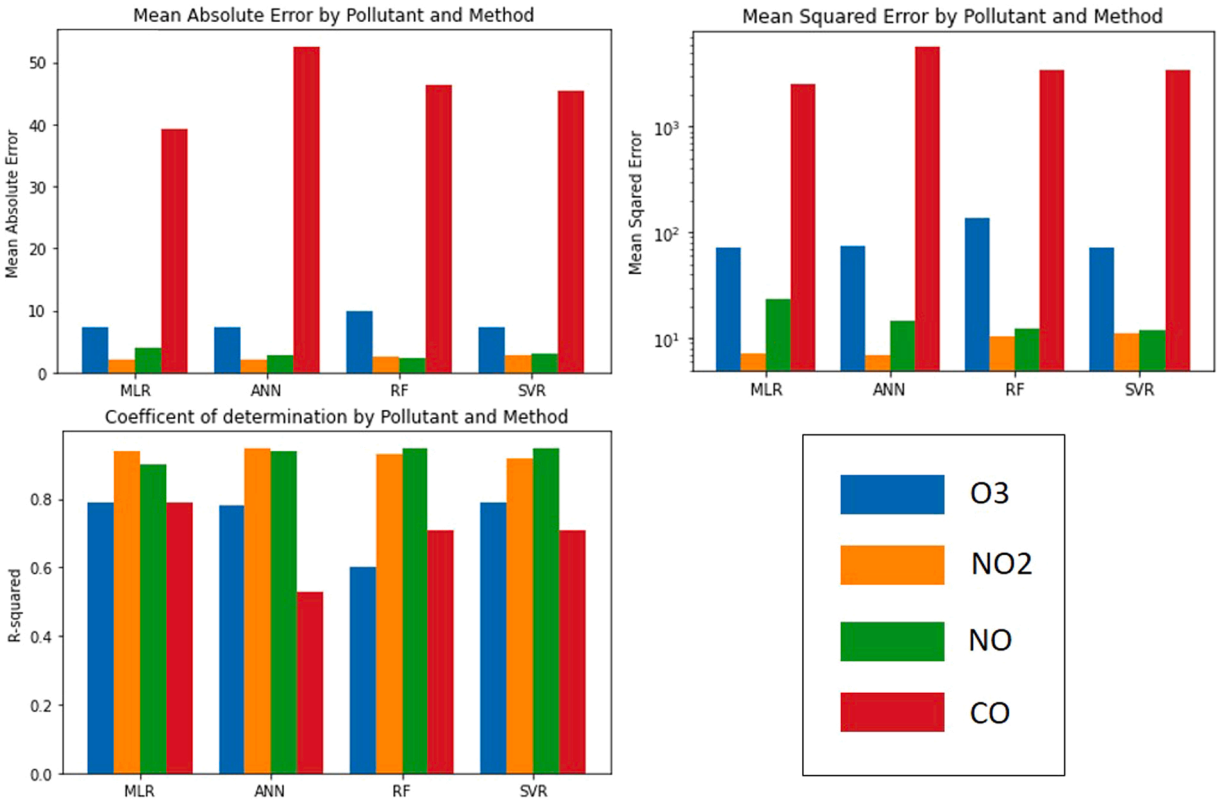

Fig. 5. Barplot of the metrics.

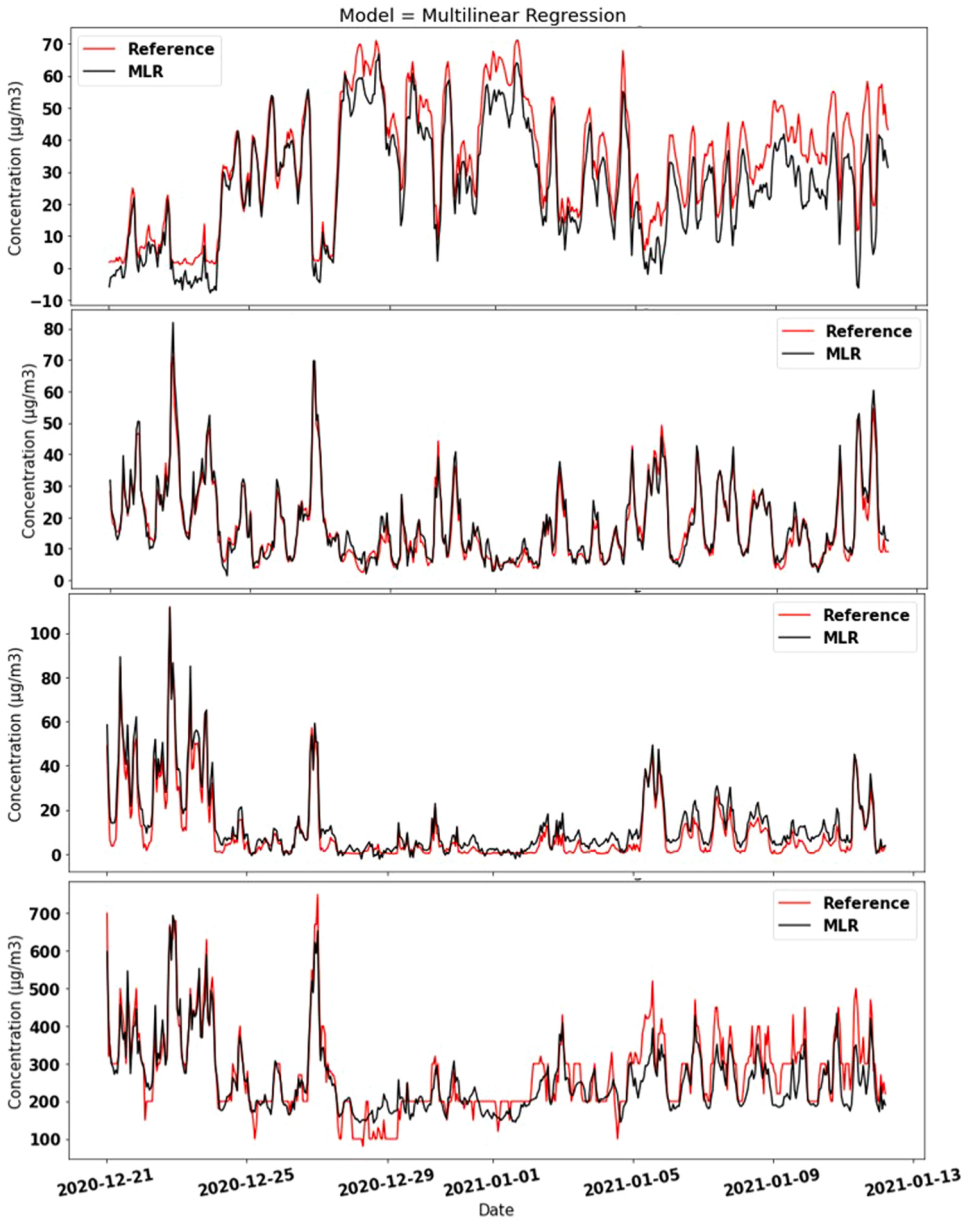

Fig. 6. Time series of each pollutant (O_3, NO_2, NO y CO) after MLR is applied.

2. Material and methods

2.1. Air quality measurement system

There are four main elements mounted on the drone: the control electronics, the gas sensors, the air sampling elements (tubes and pump) and the battery. First, the control electronics is responsible for receiving the information from the sensors and storing and/or transmitting it. The main unit is a low-power ST microcontroller based on a high-performance 32-bit core running at a frequency of up to 80 MHz. Additionally, the PCB incorporates a humidity and temperature sensor (SHT21, Sensirion) and a GPS module in order to gather more information about the environment. The data collected from all sensors is stored in a microSD every 5 s. Besides, a ZigBee (Xbee, Digi) communication module has been incorporated into the design to establish low-power wireless communication with a computer. Hence, the computer, with the XBee coordinator node connected via USB, will display in real-time the information from the sensors during the flight. For this purpose, a graphical application (Fig. 3) has been developed in Matlab which plots sensor data as it is received through the serial port (USB).

In order to measure air quality, four sensors, supplied by Alphasense, have been incorporated to detect NO_2, O_3, CO and NO. Specifically, the sensors included are OX-A431, NO2-A43F, CO-A4 and NO-A4 models. These are electrochemical sensors with four electrodes: working electrode, counter electrode, reference electrode and auxiliary electrode. An active sampling system has been included to lead the air to the sensors, thus preventing any sudden changes in pressure that could worsen sensing performance. Regarding the effects produced by downwash, several works have focused on studying this type of turbulence in multirotor UAVs [45,46]. During flight, the downflow of the rotor develops downwards in a cylindrical shape, however, beyond the propellers these turbulences disappear [47]. According to this evidence, the proposed solution to avoid turbulences caused by multirotor propellers (downwash) is to incorporate a pump with a flow rate of 280 ml/min and a 35 cm PVC tube placed horizontally on the UAV. This measurement is obtained by adding a few centimeters to the distance between the center of the UAV and the end of the propeller. In this way, the tube collects the air sample outside the field of influence of turbulence, while the pump

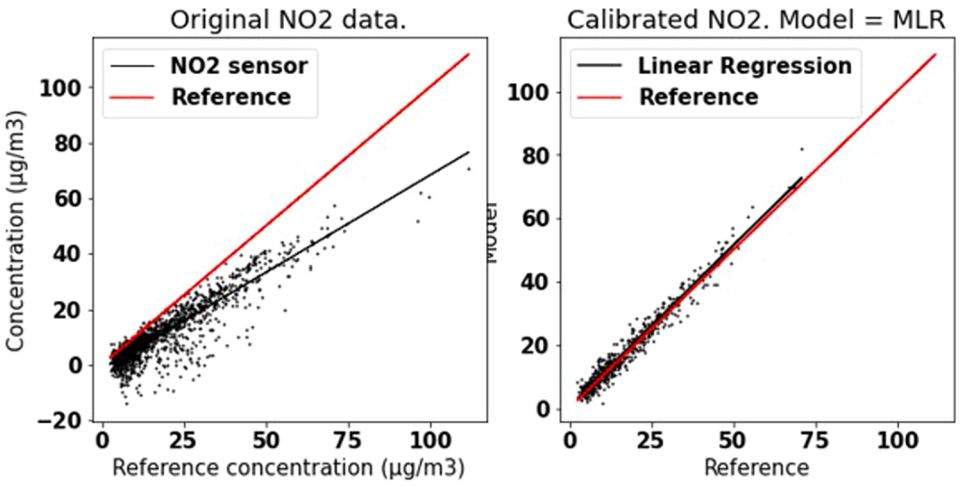

Fig. 7. NO_2 data after and before being calibrated with MLR.

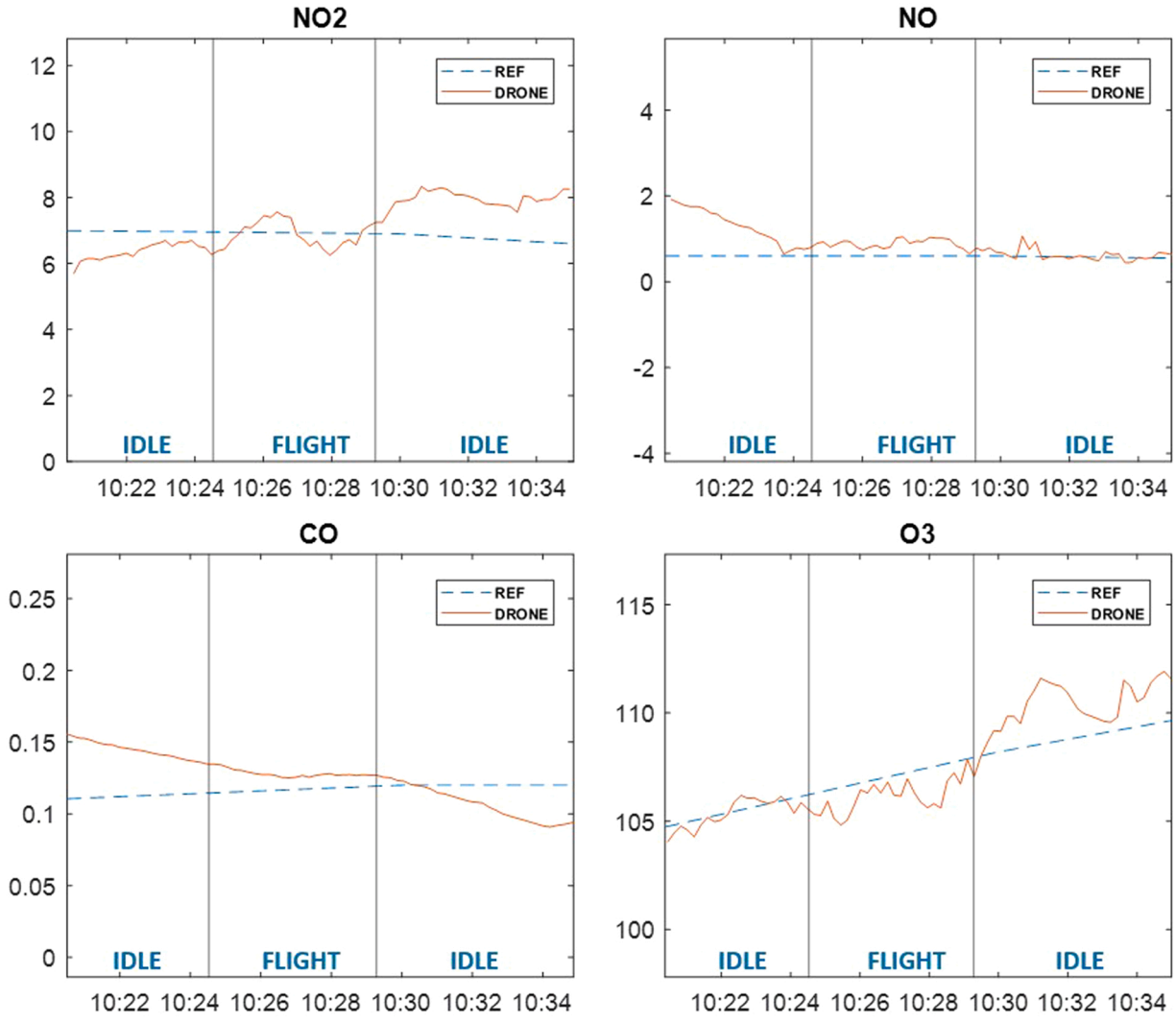

Fig. 8. Temporal variation of sensor signal during flight 1.

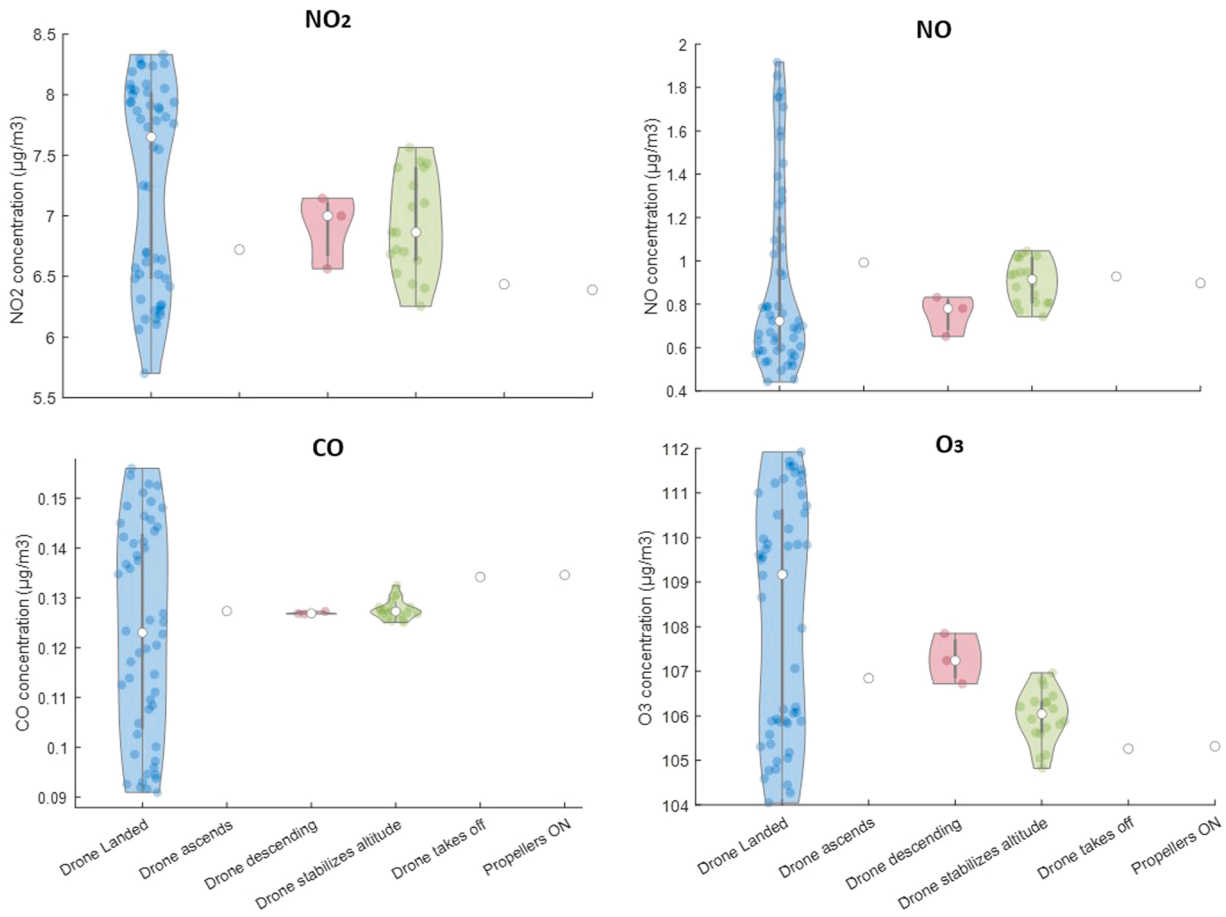

Fig. 9. Violin plot of signals during flight 1 separated by flight stage.

provides a continuous air flow that facilitates the measurement of contaminants.

Finally, the system is powered by two Li-Ion batteries of 3.7 V and 2800 mAH: one for the electronics and sensors, and another for the pump and the GPS module. Fig. 1 shows an outline of the main components that make up the sampling and air quality measurement system and Fig. 2 shows the measurement system mounted on the drone (detailing the main components).

It should be noted that, in order to avoid any electromagnetic interference from the drone, both the control electronics and the gas sensors have been shielded to isolate them. For this purpose, these two elements have been introduced into metallized boxes, thus creating Faraday cages. In this way, the electromagnetic field inside these boxes is canceled.

The weight of the complete system is approximately 750 g, so it is easily supported by the drone used without assuming a great loss of power.

2.2. UAV description and sensor integration

In this work, a hexacopter multirotor has been used with dimensions of 120 cm in diameter and 40 cm in height. The flight controller used is a PIXHAWK module that integrates a 32-bit ARM Cortex M4 core with an FPU processor. The complete system contains acceleration sensors, gyroscopes and GPS for stabilization and navigation control. Communication with the vehicle is provided with a 2.4 GHz radio channel, which allows the transmission of information up to a distance of approximately 1 Km. An additional telemetry device has also been incorporated for data communication with the ground station. In addition, the chassis structure is made of carbon fiber, which considerably decreases the weight of the vehicle, which is 2.4 kg. The vehicle, along with the measuring device, air capture and batteries, has a total weight of 3.6 kg. To obtain greater autonomy, 4-cell and 5 mAh batteries have been incorporated, enabling flights of up to 20 min. Finally, a software tool (Mission Planner) has been used for setting up the vehicle and planning the flights.

The location where the LCS device is placed in the UAV is of vital importance to make a stable flight and maintain the center of gravity. This is the reason why most of the measuring components have been placed centered on top of the vehicle in such a way that they do not affect its stability. As regards the position of the tube, it is placed over the X-axis of the vehicle, in such a way that it protrudes outside the propellers, thus avoiding most of the downwash airflows.

Fig. 3 shows a snapshot of the application programmed in Matlab for data acquisition.

2.3. Data processing - Calibration

The electrochemical sensors detailed above have been calibrated to ensure the validity of the results. To this end, a fixed reference station has been used by placing the device in parallel. It should be noted that the reference equipment used in this work belongs to the Extremadura Network for the Protection and Research of Air Quality (REPICA) of the Regional Ministry of Ecological Transition and Sustainability of the Junta de Extremadura. The equipment of which these reference stations consist is as follows.

- O_3: THERMO 49i-B3ZAA (Absortion UV)
- NO_x: THERMO 42i-BZMTPAA (chemiluminescence)
- CO: THERMO 48i-BCSAA (infrared absorption spectroscopy)

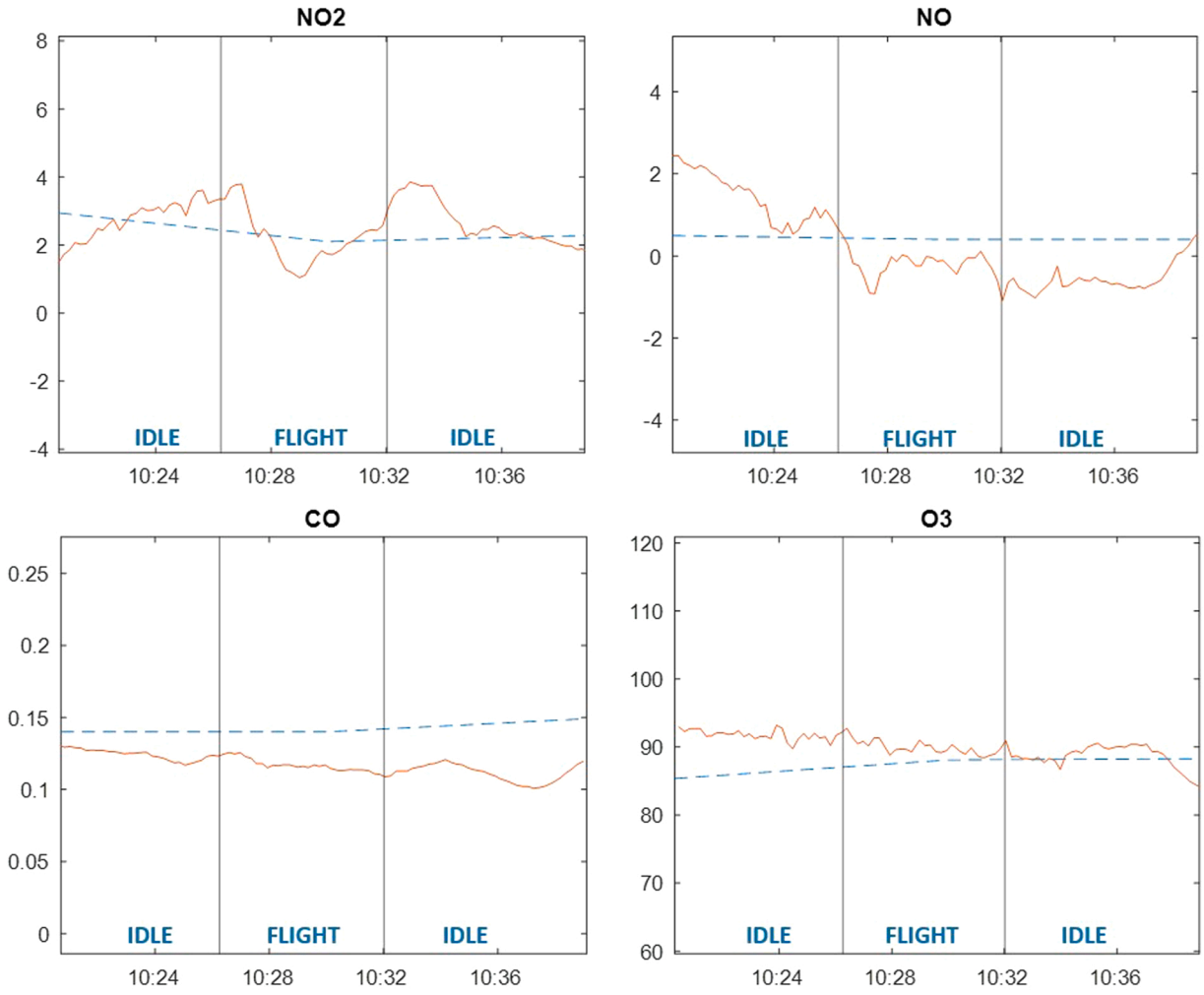

Fig. 10. Temporal variation of sensor signal during flight 2.

This equipment collects the data every ten minutes, so, in order to be able to compare the information, the data from the drone-mounted device has been averaged over periods of 10 min. Initially, as it is shown in Fig. 4, a clear deviation between concentrations measured by the sensors and the actual concentration measured at the reference station, is detected.

This deviation was attributed to the sensors being calibrated by the manufacturer under controlled laboratory conditions rather than in an outdoor environment. When working under outdoor conditions, sensor operation is affected by environmental variables, especially temperature and relative humidity [48].

To calculate the concentration, the manufacturer uses an internal algorithm that converts the values of the sensor electrodes into pollutant concentration values.

$$Pollutant(ppb) = \frac{(S_{WE} - S_{WE,0}) - n(S_{AE} - S_{AE,0})}{s} \quad (1)$$

Where S_{WE} and S_{AE} are the values of the working electrode and the auxiliary electrode respectively. $S_{WE,0}$ and $S_{AE,0}$ are the offset of the working electrode and that of the auxiliary electrode, n is a temperature-dependent parameter given by the manufacturer (from the guide tables for correction of zero background current due to temperature within the range of −30 °C to +50 °C [49]), and s is the sensitivity to the pollutant.

Fig. 4 shows that the concentration of the pollutants, calculated from the manufacturer's algorithm, do not correspond to the data measured by the reference. For this reason, it is more appropriate to work with the values of the electrodes and try to find an alternative calibration algorithm, than using the formula given by Alphasense (1). This approach is evidenced in a large number of references in the literature and it is the usual procedure that must be followed when working with this type of sensors in outdoor conditions [29,30,39,50–53].

Developing a calibration algorithm that returns the real concentration of each pollutant means replacing Eq. (1) with another one (2) that returns the gas concentration as a function of the working electrode, the auxiliary electrode (WE_i and AE_i) of each pollutant (i = NO_2, O_3, NO, CO), temperature (T) and relative humidity (RH).

$$f(WE_i, \quad AE_i, \quad T, \quad RH) = [Pollutant] \quad (2)$$

To solve this problem, Machine Learning Algorithms are usually used. In this work, four different approaches have been tested: Multiple Linear Regression, Artificial Neural Network, Support Vector Regression and Random Forest.

Machine learning techniques need a first stage of training in order to optimize their internal parameters. To optimize the algorithms a train and test set have been temporally separated. The first 60% of data corresponds to the training set, while the remaining 40% has been set aside to validate the model. These four methods are briefly described below.

2.3.1. *Multiple Linear Regression*

First, a Multiple Linear Regression (MLR) based on least-squares adjustment was implemented. This alternative seeks to express the concentration of each pollutant as a linear combination of electrode values, temperature and relative humidity. The chosen combination will

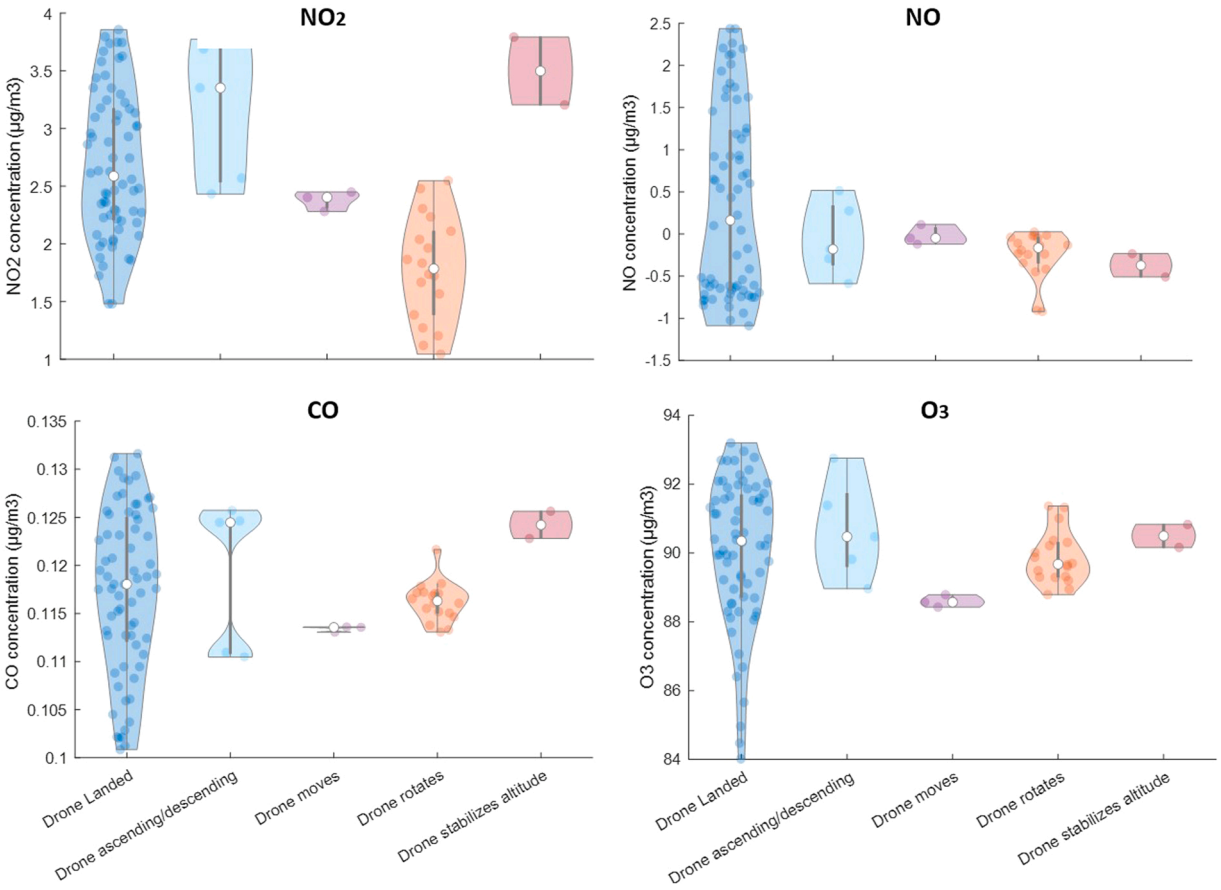

Fig. 11. Violin plot of signals during flight 2 separated by flight stage.

be one that minimizes the residuals, that is, the Euclidean distance between the calculated points and the actual value of the pollutant.

2.3.2. *Artificial Neural network*

The second method tested was an artificial neural network (ANN). In this case, a multilayer perceptron network type has been designed. A rectified linear unit has been chosen as activation function. On the other hand, as solver, we have used the stochastic gradient descent.

The optimal system obtained consists of a network composed of 10 inputs (8 electrodes, ambient temperature and relative humidity), 2 hidden layers formed by 2 neurons in each and 1 output neuron.

All this parameters have been chosen according to previous work [54] where we tested a similar procedure in order to calibrate a fix air quality monitoring station.

2.3.3. *Support Vector Regression*

Support Vector Regression (SVR) is based on a similar principle as the support vector machine (SVM) which are widely used in classification tasks, however SVR focuses on regression rather than classification [55]. This is achieved by minimizing the error condition through the so-called "linear ε-insensitive loss function". In addition, the representation by means of Kernel functions offers a non-linear problem solution, projecting the information to a space of characteristics of greater dimension which increases the computational capacity of the linear learning machines. In the implementation of the SVR, the main parameters programmed are the radial basis Kernel function and a tolerance of 10^{-3}.

2.3.4. *Random Forest*

Finally, the Random Forest (RF) technique was tested, a technique that works by implementing a large number of decision trees simultaneously.

These four techniques have been developed in Python 3.8, using the scikit-Learn 0.24.1 package.

The methods that have been described were tested and their configurations were optimized. After that, the one that showed the best results was selected as the optimal method. This selection was performed by comparing the values calculated by the algorithm with the ground truth, given by the reference station. To compare, statistical indices such as the coefficient of determination (R^2), mean absolute error (MAE) and mean square error (MSE), were calculated.

2.4. *Experimental development*

To validate the system, two different types of measurements have been carried out: static and in-flight. All the tests have been carried out in the area of Badajoz (Extremadura, Spain).

Static measurements have been used to calibrate the gas sensors before performing measurements in motion. This phase is of great importance in the use of this type of sensor since, apart from correcting possible offset and slope effects, it is essential to correct the effects derived from changes in temperature and humidity. These calibration measurements have been carried out in a central area of the city because higher concentrations are reached there, thus allowing better performance of the algorithms. The device has been placed in parallel with a mobile reference station for approximately two months (from November 16, 2020, to January 20, 2021).

Once the algorithm for calibration and correction of the data has been created and implemented, flight tests are performed. The flight tests seek, first of all, to verify that the operation of the drone does not affect the behavior of the sensors. Therefore, two short flights (approximately 5 min) have been performed and observed for

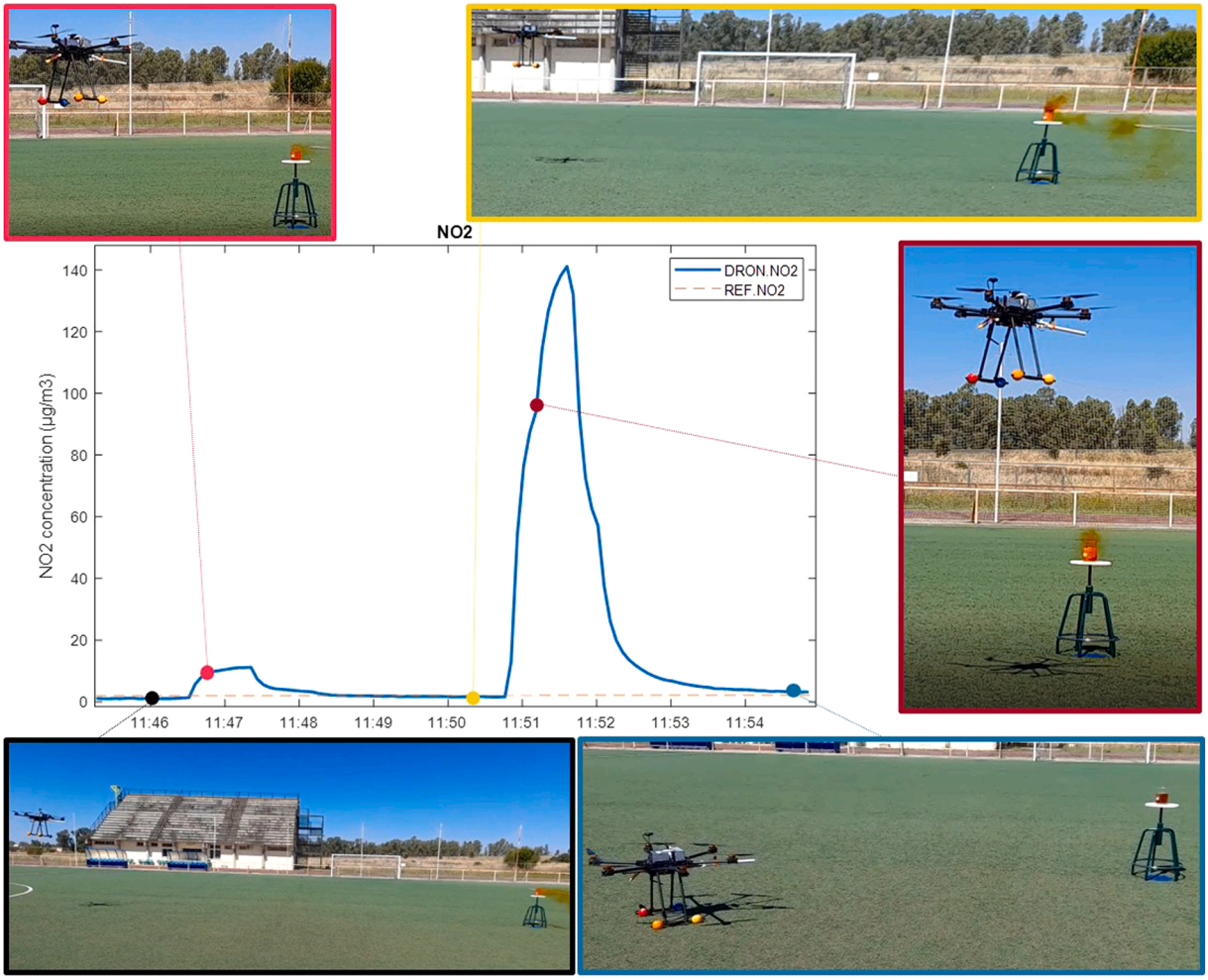

Fig. 12. Line chart of NO_2 signal from the NO2-A43F sensor throughout the flight along with the actual concentration signal from the reference station.

disturbances in sensor signals caused by the movement of the drone. Next, the ability of the device to react to changes in concentration and locate sources of contamination is checked. For this purpose, another flight has been completed around an artificial source of NO_2. This source was originated from the reaction between nitric acid and copper:

$$4HNO_3 + Cu \rightarrow Cu(NO_3)_2 + 2NO_2 + 2H_2O \quad (3)$$

As can be seen in expression (3), the acid reacts with copper forming nitrogen dioxide (reddish-brown gas) as well as copper nitrate and water. In this way, it is possible to visualize the NO_2 cloud at all times. Finally, it should be noted that these flights have been performed in a non-central area, 80 m away from a fixed reference station, which allows the actual concentrations of pollutants to be checked during the flight.

3. Results and discussion

3.1. Static measurements

In this section, the static measures and the calibration results are presented. First, the values of the three statistics (MAE, MSE and R^2) are shown in table format (Table 1) along with the average value of each pollutant before calibration. It can be seen that MAE and MSE values are higher in the case of CO. This occurs according to expected because CO concentration was higher than the concentration for the other three pollutants in the period in which the tests were carried out. This is appreciated by seeing the mean value.

Table 2 shows the three metrics that evaluate the model when applying each of the four techniques described in Section 2.3. Green highlights which algorithm is giving the best results for each pollutant and for each metric. For example, Neural Network is the one with the lowest mean absolute error. However, mean squared error and R^2 are better in the case of Multiple Linear Regression. Fig. 5 shows a barplot in which the information in Table 2 is summarized. These results suggest that multiple linear regression is the algorithm that works best when it comes to obtaining an estimated value of the concentration, especially in the case of NO_2 and O_3. This technique gives the highest values for the coefficient of determination, while maintaining relatively low values of MAE and MSE compared to the other three algorithms. Time series for each pollutant are shown in Fig. 6 when a correction based on multiple linear regression is applied.

As shown in Table 2 and Fig. 5, the coefficient of determination (R^2) is lower in the case of CO than in the rest of the pollutants. This deviation is mainly related to the unit of measurement of the reference for CO. The reference station used during static tests measures CO concentration in mg/m^3, while NO_2, O_3 and NO concentration were measured in $\mu g/m^3$, which implies a lower resolution in CO data. This loss of precision in the original data means less accuracy after calibration.

Finally, Fig. 7 shows an overall better performance when it comes to the NO and NO_2 series, with low values of MAE and MSE and reaching R^2 values of up to 0.95.

In summary, despite the low initial correlation between reference equipment and sensors and the CO data format, multiple linear regression calibration allows time series to be adjusted and much more reliable

data to be obtained. This calibration was applied to the sensors before in-flight measurements to ensure data quality.

3.2. In-flight measurements

The flight test results are intended to verify that the movement of the drone does not interfere with sensor signals. For this purpose, two flights of the drone were carried out with the measuring device mounted on it. In the first flight, the drone only takes off and stabilizes at a flight height of 2 m for several minutes to finally ascend to 3 m and then land. Fig. 8 shows the temporal variation of each of the sensor signals during, before, and after the flight. Thereby, we compare the behavior of the signal in flight and idle (landed with the propellers deactivated). Although there are variations in the signals, they do not seem to increase significantly during the flight. On these graphs, the ten-minute value of the reference station has also been depicted for that period.

When representing the signals of each phase of flight in a violin diagram, it can be found that pollutant concentration values do not reach different values than those reached while the drone is landed and idle (Fig. 9). Therefore, it can be inferred that the coupled gas monitoring system is not significantly affected by the downwash and the vertical movements of the drone.

A second flight, in which the drone performs rotational and translational movements, was carried out to verify the correct performance of the system. Outlining the flight procedure, from 10:27:00 the drone rotates 720º constantly for approximately 3 min and 40 s. At 10:31:00 the drone moves forward for 25 s and immediately backs up to the same starting point without rotation. Fig. 10 shows that the temporary signal in the case of the NO_2 sensor creates a valley during the flight. Since no similar disturbance appears in the rest of the sensors, it is not likely to be a consequence of the movement of the drone and could be considered to be due to a real variation in the concentration of NO_2 in the environment. Even so, the variation of the signal is of the order of 2 µg/m3, so it is not of great relevance. As before, when representing the violin diagrams (Fig. 11), it can be observed that the variation of the data is not significant with respect to the variation of pollution found in the air (variation while the drone is landed).

On the other hand, the results obtained in the last flight, carried out with a nearby NO_2 source, are shown. Fig. 12 shows the temporal graph of the NO_2 signal from the NO2-A43F sensor throughout the flight along with the actual concentration signal from the reference station. The graph is accompanied by some screenshots of some of the key moments of the test. The main stages of the flight are detailed below. At 11:45:30 the flight begins at 23 m distance from the NO_2 source. At 11:46:36 the drone approaches within 2 m of the source, although the reaction generated is ending and the NO_2 cloud generated is barely perceptible. At 11:47:26 the drone moves away from the source again up to 23 m and the chemical reaction is reactivated providing more copper. At 11:50:10 it starts to approach the source, reaching again a distance below 2 m at approximately 11:50:56 and the sampling tube is positioned in the vertical of the beaker. At 11:51:31 the drone moves away from the source of NO_2 and it is observed that the signal descends. At 11:52:26 the drone approaches the source for the last time, but the chemical reaction seems to have ended. At 11:54:51 the drone is landed. Concerning the signal of the reference station, it does not suffer great variations because it is located 80 m from the NO_2 source. In addition, as detailed above, these data are averaged every ten minutes. It is observed that when the drone is close to the NO_2 source and it is active, the NO2-A43F sensor responds quickly and noticeably.

4. Conclusions and future trends

In this work, we present the development of an unmanned aerial vehicle with an electronic system for real-time air pollution monitoring by means of mobile intelligent detection in areas with little or no accessibility. The device incorporates a high-precision measurement system with sensors for measuring O3, NO, NO2, and CO. In addition, monitoring data is available as real-time information.

The main conclusion of this experiment is that the presented prototype can be used for pollutant detection and air quality monitoring with an accuracy of up to 0.95 (R^2) for NO_2 and NO pollutants. The system has been calibrated by evaluating different techniques based on machine learning. A major finding of this work is that, with the sampling and isolation system developed, the monitoring device is not affected at any time by the movement of the drone, the downwash effect or electromagnetic disturbances.

Future work will consider the possibility of carrying out more field tests and longer flights that will provide additional insight into the behavior of the system.

CRediT authorship contribution statement

Patricia Arroyo: Methodology, Resources, Writing – original draft, Writing – review & editing, **Gomez Jaime Gómez:** Validation, Formal analysis, Data curation, Writing – review & editing, Visualization, **José Luis Herrero:** Software, Supervision, **Jesus Lozano:** Conceptualization, Investigation, Project administration, Funding acquisition.

Declaration of Competing Interest

The authors declare that they have no known competing financial interests or personal relationships that could have appeared to influence the work reported in this paper.

Acknowledgments

Authors want to thank European Union through Interreg-Sudoe program for supporting NanoSen-AQM project (SOE/P1/E0569) and Spanish Ministry of Science, Innovation and Universities for supporting the NEOGAS project (PID2019-107697RB-C44).

References

[1] I. Manisalidis, E. Stavropoulou, A. Stavropoulos, E. Bezirtzoglou, Environmental and health impacts of air pollution: a review, Front. Public Health 8 (2020), https://doi.org/10.3389/fpubh.2020.00014.
[2] SIGNALS 2020 - Towards Zero Pollution in Europe, in: N.d. In, n.d. https://doi.org/⟨https://doi.org/10.2800/40627⟩.
[3] J. Lelieveld, J.S. Evans, M. Fnais, D. Giannadaki, A. Pozzer, The contribution of outdoor air pollution sources to premature mortality on a global scale, Nature 525 (2015) 367–371, https://doi.org/10.1038/nature15371.
[4] P.J. Landrigan, Air pollution and health, Lancet Public Health 2 (2017) e4–e5, https://doi.org/10.1016/S2468-2667(16)30023-8.
[5] B. Brunekreef, S.T. Holgate, Air pollution and health, Lancet 360 (2002) 1233–1242, https://doi.org/10.1016/S0140-6736(02)11274-8.
[6] Y. Zhang, R. Ma, J. Ban, F. Lu, M. Guo, Y. Zhong, N. Jiang, C. Chen, T. Li, X. Shi, Risk of cardiovascular hospital admission after exposure to fine particulate pollution, J. Am. Coll. Cardiol. 78 (2021) 1015–1024, https://doi.org/10.1016/j.jacc.2021.06.043.
[7] S.Y. Kim, S.H. Kim, J.H. Wee, C. Min, S.-M. Han, S. Kim, H.G. Choi, Short and long term exposure to air pollution increases the risk of ischemic heart disease, Sci. Rep. 11 (2021) 5108, https://doi.org/10.1038/s41598-021-84587-x.
[8] S. Shin, L. Bai, R.T. Burnett, J.C. Kwong, P. Hystad, A. van Donkelaar, E. Lavigne, S. Weichenthal, R. Copes, R. v Martin, A. Kopp, H. Chen, Air pollution as a risk factor for incident chronic obstructive pulmonary disease and asthma. A 15-year population-based cohort study, Am. J. Respir. Crit. Care Med. 203 (2021) 1138–1148, https://doi.org/10.1164/rccm.201909-1744OC.

[9] D. Clofent, M. Culebras, K. Loor, M.J. Cruz, Contaminación ambiental y cáncer de pulmón: el poder carcinogénico del aire que respiramos, Arch. Bronconeumol. 57 (2021) 317–318, https://doi.org/10.1016/j.arbres.2020.05.031.
[10] F. Hu, L. Jing, R. Shi, Analysis of related factors and disease costs of respiratory infection and environmental pollution in children, Technol. Health Care 28 (2020) 355–360, https://doi.org/10.3233/THC-209036.
[11] V. Lambey, A.D. Prasad, A review on air quality measurement using an unmanned aerial vehicle, Water Air Soil Pollut. 232 (2021) 109, https://doi.org/10.1007/s11270-020-04973-5.
[12] X.-B. Li, D.-S. Wang, Q.-C. Lu, Z.-R. Peng, Z.-Y. Wang, Investigating vertical distribution patterns of lower tropospheric PM2.5 using unmanned aerial vehicle measurements, Atmos. Environ. 173 (2018) 62–71, https://doi.org/10.1016/j.atmosenv.2017.11.009.
[13] Z. Tao, Z. Wang, S. Yang, H. Shan, X. Ma, H. Zhang, S. Zhao, D. Liu, C. Xie, Y. Wang, Profiling the PM2.5 mass concentration vertical distribution in the boundary layer, Atmos. Meas. Tech. 9 (2016) 1369–1376, https://doi.org/10.5194/amt-9-1369-2016.
[14] J.-B. Renard, V. Michoud, J. Giacomoni, Vertical profiles of pollution particle concentrations in the boundary layer above Paris (France) from the optical aerosol counter LOAC onboard a touristic balloon, Sensors 20 (2020) 1111, https://doi.org/10.3390/s20041111.
[15] H. Sun, Y. Shi, L. Liu, W. Ding, Z. Zhang, F. Hu, Impacts of atmospheric boundary layer vertical structure on haze pollution observed by tethered balloon and lidar, J. Meteorol. Res. 35 (2021) 209–223, https://doi.org/10.1007/s13351-021-0076-4.
[16] T. Villa, F. Gonzalez, B. Miljievic, Z. Ristovski, L. Morawska, An overview of small unmanned aerial vehicles for air quality measurements: present applications and future prospectives, Sensors 16 (2016) 1072, https://doi.org/10.3390/s16071072.
[17] M. Sorek-Hamer, R. Chatfield, Y. Liu, Review: strategies for using satellite-based products in modeling PM2.5 and short-term pollution episodes, Environ. Int. 144 (2020), 106057, https://doi.org/10.1016/j.envint.2020.106057.
[18] C. Brosy, K. Krampf, M. Zeeman, B. Wolf, W. Junkermann, K. Schäfer, S. Emeis, H. Kunstmann, Simultaneous multicopter-based air sampling and sensing of meteorological variables, Atmos. Meas. Tech. 10 (2017) 2773–2784, https://doi.org/10.5194/amt-10-2773-2017.
[19] J.O. Araujo, J. Valente, L. Kooistra, S. Munniks, R.J.B. Peters, Experimental flight patterns evaluation for a UAV-based air pollutant sensor, Micromachines 11 (2020) 768, https://doi.org/10.3390/mi11080768.
[20] S.D. Zhi, Y.B. Wei, Z.H. Yu, Air Quality Monitoring Platform based on Remote Unmanned Aerial Vehicle with Wireless Communication, in: Proceedings of the International Conference on Future Networks and Distributed Systems, ACM, New York, NY, USA, 2017: pp. 1–7. https://doi.org/10.1145/3102304.3102339.
[21] S. Pochwała, A. Gardecki, P. Lewandowski, V. Somogyi, S. Anweiler, Developing of low-cost air pollution sensor—measurements with the unmanned aerial vehicles in Poland, Sensors 20 (2020) 3582, https://doi.org/10.3390/s20123582.
[22] Q. Chen, X.-B. Li, R. Song, H.-W. Wang, B. Li, H.-D. He, Z.-R. Peng, Development and utilization of hexacopter unmanned aerial vehicle platform to characterize vertical distribution of boundary layer ozone in wintertime, Atmos. Pollut. Res. 11 (2020) 1073–1083, https://doi.org/10.1016/j.apr.2020.04.002.
[23] T.F. Villa, R.A. Brown, E.R. Jayaratne, L.F. Gonzalez, L. Morawska, Z.D. Ristovski, Characterization of the particle emission from a ship operating at sea using an unmanned aerial vehicle, Atmos. Meas. Tech. 12 (2019) 691–702, https://doi.org/10.5194/amt-12-691-2019.
[24] C.-C. Chang, C.-Y. Chang, J.-L. Wang, X.-X. Pan, Y.-C. Chen, Y.-J. Ho, An optimized multicopter UAV sounding technique (MUST) for probing comprehensive atmospheric variables, Chemosphere 254 (2020), 126867, https://doi.org/10.1016/j.chemosphere.2020.126867.
[25] G. Rohi, O. Ejofodomi, G. Ofualagba, Autonomous monitoring, analysis, and countering of air pollution using environmental drones, Heliyon 6 (2020), e03252, https://doi.org/10.1016/j.heliyon.2020.e03252.
[26] A.C. Lewis, E. von Schneidemesser, R.E. Peltier, Low-cost sensors for the measurement of atmospheric composition: overview of topic and future applications valid as of May 2018, n.d.
[27] F. Karagulian, M. Barbiere, A. Kotsev, L. Spinelle, M. Gerboles, F. Lagler, N. Redon, S. Crunaire, A. Borowiak, Review of the performance of low-cost sensors for air quality monitoring, Atmosphere 10 (2019) 506, https://doi.org/10.3390/atmos10090506.
[28] A.C. Rai, P. Kumar, F. Pilla, A.N. Skouloudis, S. di Sabatino, C. Ratti, A. Yasar, D. Rickerby, End-user perspective of low-cost sensors for outdoor air pollution monitoring, Sci. Total Environ. 607–608 (2017) 691–705, https://doi.org/10.1016/j.scitotenv.2017.06.266.
[29] J.M. Cordero, R. Borge, A. Narros, Using statistical methods to carry out in field calibrations of low cost air quality sensors, Sens. Actuators B Chem. 267 (2018) 245–254, https://doi.org/10.1016/j.snb.2018.04.021.
[30] S. de Vito, E. Esposito, M. Salvato, O. Popoola, F. Formisano, R. Jones, G. di Francia, Calibrating chemical multisensory devices for real world applications: An in-depth comparison of quantitative machine learning approaches, Sens. Actuators B Chem. 255 (2018) 1191–1210, https://doi.org/10.1016/j.snb.2017.07.155.
[31] J. Burgués, S. Marco, Feature extraction for transient chemical sensor signals in response to turbulent plumes: application to chemical source distance prediction, Sens. Actuators B Chem. 320 (2020), 128235, https://doi.org/10.1016/j.snb.2020.128235.
[32] M. Alvarado, F. Gonzalez, A. Fletcher, A. Doshi, Towards the development of a low cost airborne sensing system to monitor dust particles after blasting at open-pit mine sites, Sensors 15 (2015) 19667–19687, https://doi.org/10.3390/s150819667.
[33] M. Carrozzo, S. de Vito, E. Esposito, M. Salvato, F. Formisano, E. Massera, G. di Francia, P.D. Veneri, M. Iadaresta, A. Mennella, UAV Intelligent Chemical Multisensor Payload for Networked and Impromptu Gas Monitoring Tasks, in: 2018 5th IEEE International Workshop on Metrology for AeroSpace (MetroAeroSpace), IEEE, 2018: pp. 112–116. https://doi.org/10.1109/MetroAeroSpace.2018.8453543.
[34] J. Burgués, S. Marco, Environmental chemical sensing using small drones: a review, Sci. Total Environ. 748 (2020), 141172, https://doi.org/10.1016/j.scitotenv.2020.141172.
[35] Q. Gu, D.R. Michanowicz, C. Jia, Developing a modular unmanned aerial vehicle (UAV) platform for air pollution profiling, Sensors 18 (2018) 4363, https://doi.org/10.3390/s18124363.
[36] A. Shen, S. Zhou, S. Peng, Atmospheric environment detection method based on multi-rotor UAV platform, Int. Arch. Photogramm., Remote Sens. Spat. Inf. Sci. XLII-3/W5 (2018) 67–71, https://doi.org/10.5194/isprs-archives-XLII-3-W5-67-2018.
[37] C. Li, W. Han, M. Peng, M. Zhang, X. Yao, W. Liu, T. Wang, An unmanned aerial vehicle-based gas sampling system for analyzing CO_2 and atmospheric particulate matter in laboratory, Sensors 20 (2020) 1051, https://doi.org/10.3390/s20041051.
[38] J. Valente, S. Munniks, I. de Man, L. Kooistra, Validation of a small flying e-nose system for air pollutants control: A plume detection case study from an agricultural machine, in: 2018 IEEE International Conference on Robotics and Biomimetics (ROBIO), IEEE, 2018: pp. 1993–1998. https://doi.org/10.1109/ROBIO.2018.8664718.
[39] R. Mawrence, S. Munniks, J. Valente, Calibration of electrochemical sensors for nitrogen dioxide gas detection using unmanned aerial vehicles, Sensors 20 (2020) 7332, https://doi.org/10.3390/s20247332.
[40] Y. Wu, L. Qi, H. Zhang, E.M. Musiu, Z. Yang, P. Wang, Design of UAV downwash airflow field detection system based on strain effect principle, Sensors 19 (2019) 2630, https://doi.org/10.3390/s19112630.
[41] Y. Lei, M. Cheng, Aerodynamic performance of Hex-Rotor UAV considering the horizontal airflow, Appl. Sci. 9 (2019) 4797, https://doi.org/10.3390/app9224797.
[42] J. Burgués, V. Hernández, A. Lilienthal, S. Marco, Smelling nano aerial vehicle for gas source localization and mapping, Sensors 19 (2019) 478, https://doi.org/10.3390/s19030478.
[43] C. Ercolani, A. Martinoli, 3D Odor Source Localization using a Micro Aerial Vehicle: System Design and Performance Evaluation, in: 2020 IEEE/RSJ International Conference on Intelligent Robots and Systems (IROS), IEEE, 2020: pp. 6194–6200. https://doi.org/10.1109/IROS45743.2020.9341501.
[44] F. Yang, X. Xue, C. Cai, Z. Sun, Q. Zhou, Numerical simulation and analysis on spray drift movement of multirotor plant protection unmanned aerial vehicle, Energies 11 (2018) 2399, https://doi.org/10.3390/en11092399.
[45] H. Zhang, L. Qi, Y. Wu, E.M. Musiu, Z. Cheng, P. Wang, Numerical simulation of airflow field from a six–rotor plant protection drone using lattice Boltzmann method, Biosyst. Eng. 197 (2020) 336–351, https://doi.org/10.1016/j.biosystemseng.2020.07.018.
[46] Z. Fu, Y. Chen, Y. Ding, D. He, Pollution source localization based on multi-UAV cooperative communication, IEEE Access 7 (2019) 29304–29312, https://doi.org/10.1109/ACCESS.2019.2900475.
[47] Q. Guo, Y. Zhu, Y. Tang, C. Hou, Y. He, J. Zhuang, Y. Zheng, S. Luo, CFD simulation and experimental verification of the spatial and temporal distributions of the downwash airflow of a quad-rotor agricultural UAV in hover, Comput. Electron. Agric. 172 (2020), 105343, https://doi.org/10.1016/j.compag.2020.105343.
[48] H.-Y. Liu, P. Schneider, R. Haugen, M. Vogt, Performance assessment of a low-cost PM2.5 sensor for a near four-month period in Oslo, Norway, Atmosphere 10 (2019) 41, https://doi.org/10.3390/atmos10020041.
[49] Alphasense Ltd, Alphasense Application Note - AAN 803–05, Great Notley, Essex (UK), 2019.
[50] B. Mijling, Q. Jiang, D. de Jonge, S. Bocconi, Field calibration of electrochemical NO₂ sensors in a citizen science context, Atmos. Meas. Tech. 11 (2018) 1297–1312, https://doi.org/10.5194/amt-11-1297-2018.
[51] V. van Zoest, F.B. Osei, A. Stein, G. Hoek, Calibration of low-cost NO2 sensors in an urban air quality network, Atmos. Environ. 210 (2019) 66–75, https://doi.org/10.1016/j.atmosenv.2019.04.048.
[52] P. Han, H. Mei, D. Liu, N. Zeng, X. Tang, Y. Wang, Y. Pan, Calibrations of low-cost air pollution monitoring sensors for CO, NO2, O3, and SO2, Sensors 21 (2021) 256, https://doi.org/10.3390/s21010256.
[53] M.-E. Ionascu, N. Castell, O. Boncalo, P. Schneider, M. Darie, M. Marcu, Calibration of CO, NO2, and O3 using airify: a low-cost sensor cluster for air quality monitoring, Sensors 21 (2021) 7977, https://doi.org/10.3390/s21237977.
[54] P. Arroyo, J. Gómez-Suárez, J.I. Suárez, J. Lozano, Low-cost air quality measurement system based on electrochemical and PM sensors with cloud connection, Sensors 21 (2021) 6228, https://doi.org/10.3390/s21186228.
[55] R. Laref, E. Losson, A. Sava, M. Siadat, R. Laref, E. Losson, A. Sava, M. Siadat, Support vector machine regression for calibration transfer between electronic noses dedicated to air pollution monitoring, Sensors 18 (2018) 3716, https://doi.org/10.3390/s18113716.

Patricia Arroyo received his B.Sc. M. Sc. and Ph. D. in Electronic Engineering from the University of Extremadura. She is currently a postdoctoral researcher at the Industrial Engineering School. His research interests include chemical sensors, electronic instrumentation and machine learning.

Jaime Gómez-Suárez received his B.Sc. in physics from the University of Extremadura. He is currently pursuing the Ph.D. degree with the Industrial Engineering School. His work focuses on the calibration of low-cost sensors for air quality monitoring. His research interests include artificial intelligence and machine learning.

José Luis Herrero received his B.Sc. in computer science from the University of Granada and his Ph. D. from the University of Extremadura. He is currently Associate professor at the Industrial Engineering School. His research interests include Unmanned Aerial Vehicles, artificial intelligence and programming.

Jesús Lozano received the B. Sc. degree in Electronic Engineer in 2001 and Ph. D. degree in 2005 from Universidad Complutense de Madrid (UCM), Spain. He has been a researcher at the UCM, Consejo Superior de Investigaciones Científicas and Universidad Politécnica de Madrid. Presently he works as full professor at the Industrial Engineering School of Universidad de Extremadura, Badajoz. His research interests include pattern recognition techniques, machine olfaction, intelligent systems and chemical sensors.